# Global behaviour of a composite stiffened panel in buckling. Part 1: Numerical modelling

Adrien Perret, Sebastien Mistou, Marina Fazzini

# Global behaviour of a composite stiffened panel in buckling. Part 1: Numerical modelling

Adrien Perret [a,b,*], Sébastien Mistou [b], Marina Fazzini [b]

[a] DAHER-SOCATA, Aéroport Tarbes-Lourdes-Pyrénées, 65290 Louey, France
[b] ENIT-LGP, PRES Université de Toulouse, Av. Azereix, BP1629, 65016 Tarbes, France

*Keywords:*
Structural composites
Fracture
Buckling
Failure criterion
Modelling

A B S T R A C T

The present study analyses an aircraft composite fuselage structure manufactured by the Liquid Resin Infusion (LRI) process and subjected to a compressive load. LRI is based on the moulding of high performance composite parts by infusing liquid resin on dry fibres instead of prepreg fabrics or Resin Transfer Moulding (RTM). Actual industrial projects face composite integrated structure issues as a number of structures (stiffeners, ...) are more and more integrated onto the skins of aircraft fuselage. A representative panel of a composite fuselage to be tested in buckling is studied numerically.

This paper studies which of the real behaviours of the integrated structures are to be observed during this test. Numerical models are studied at a global scale of the composite stiffened panel. Linear and non linear analyses are conducted. The Tsai–Wu criterion with a progressive failure analysis is implemented, to describe the global behaviour of the panel up to collapse. Also, three stiffener connection methods are compared at the intersection between two types of integrated structures. Load shortening curves permit to estimate the expected load and displacements.

## 1. Introduction

As composite components are evolving in the aerospace industry, one of their main advantages is to integrate co-bonded or co-cured structures. Many recent studies can be found concerning the investigation of these concepts into the application of composite fuselage structures. TANGO [1] was the first program in Europe to study a pressurised composite fuselage demonstrator leading to a full scale test of an A321 type fuselage section. This fuselage was made from frames and stringers and was dedicated to commercial transport aircraft. POSICOSS program [2] was undertaken at the same time as TANGO, but was followed by COCOMAT program [3] which undertook deeper studies of the dimensioning methods. These study were mostly dedicated to increase the onset of degradation allowed during post-buckling of composite stiffened panels above the ultimate load.

Comparison between several composite panel finite element models made of prepregs exist [4] using Nastran and Abaqus solvers and take into account geometrical imperfections and a stress-based degradation methodology applied to the adhesive layer at the skin–stiffener interface. These authors also explain how delamination occurs [5] and implement a global–local approach where the deformation field of a global shell model is incorporated at the boundary conditions of a three-dimensional model of a skin–stiffener interface. The first step is to locate initiation of inter or intra laminar damage with a stress-based criterion. A strain-based criterion could also be used at this step along with the Strain Invariant Failure Theory (SIFT) [6]. Then an interlaminar damage growth is implemented in a second step, and Virtual Crack Closure Technique (VCCT) [7,8] is used to determine the onset of propagation with the Benzeggagh–Kenane (B–K) criterion [9]. However this global–local approach has been applied by other authors to hat shaped [10–12] or T-shaped [13,14] stringers by using the B–K criterion at the skin–stiffener interface and on 3D local models.

Globally it has been observed that considering strain energy release rate criteria in order to describe a delamination problem at the skin–stiffener interface is a good approach to substantiate the debonding behaviour of the usual integrated structures made of prepregs.

The presented Finite Element Analysis (FEA) models concern a global model to study the global behaviour of a panel, that does not need to consider an adhesive layer at the skin–stiffener interface. Moreover, the whole structure is industrially manufactured at the same time by the LRI process. The failure can initiate anywhere through the thickness, rather than the damage initiated at the interface. The Tsai–Wu stress-based criterion [15] is

* Corresponding author. Address: Laboratoire Génie de Production, École Nationale d'Ingénieurs de Tarbes, Équipe Mécanique des Matériaux, des Structures et Procédés (M2SP), Av. Azereix, BP1629, 65016 Tarbes, France. Tel.: +33 5 62 44 27 00.
*E-mail address:* Adrien.Perret@enit.fr (A. Perret).

implemented to describe the progressive failure of the structure and the composite stiffened panel is considered as being made up by a fabric stacking sequence.

This study helps to set up a compressive experimental test of the studied composite stiffened panel. Several authors have developed more or less complicated test methods. Some authors have investigated a test where composite fuselage panels are subjected to pressurisation combined with axial compression conditions [16]. Simpler test methods concern shear test [12,14] and compression test with clamped edges [12,17]. The difficulties arising from the simulation of the lateral edges being more and more constrained as the panel buckles, have led some authors to investigate several modelling approaches using spring elements to fit numerical results with experimental ones [17]. As a result the removing of lateral boundary conditions for the lateral stiffeners to insure a rigidity to the panel's edges has been looked into.

## 2. Methodologies

The methodologies described below outline how the studied composite stiffened panel is modeled. In the manufacturing process four sub-structure areas define the model. They will be referred to as the skin, the stiffeners, two fabric tapes and the transverse structures as shown in Fig. 1. These areas make a fuselage representative structure with its skin, stringers and frames. The two fabric tapes are additional fabric plies in the vicinity of the transverse structures which are located between the skin and the transverse structures.

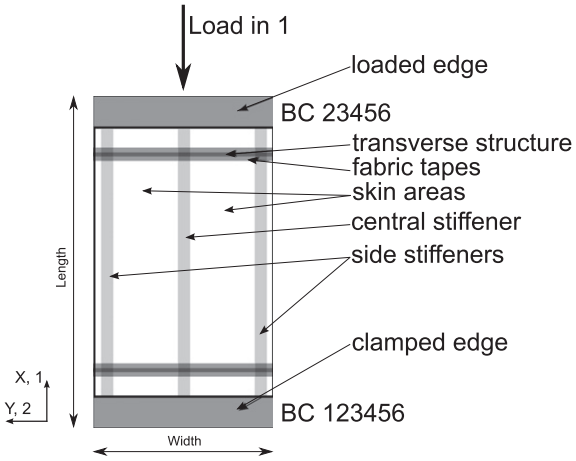


**Fig. 1.** The composite stiffened panel.

### 2.1. Analysis method

The pre- and post-processing tool of these analyses is MSC.Patran (Patran). The solver is MSC.Nastran (Nastran) for linear analysis with SOL101 (linear analysis) and SOL105 (linear buckling). MSC.Marc solver (Marc) is used for implicit non linear analysis called by the Nastran solver with SOL600, Newton–Raphson method is used with a residual force of 0.1.

Around the current analyses four aspects will be discussed. These are panel geometry, outcomes of using a linear analysis, displacements to be applied to a non linear analysis, and influence of the choice of a connection method between integrated structures. Table 1 summarises these characteristics and gives a specific order to the studied models as well as a means for referencing panels in the text. The Reference number refers to the numbering of each panel model. The first number depends on the analysis applied to the model. The second number corresponds to the boundary condition, the geometry, the material properties and the connection method, that define the model. Two sets of material properties are used. The first set concerns models 1.x, 2.x and 3.x and is given in this paper. The second set is used for models 4.x. It is an industrial set and is not given in this paper. The connection method is related to how the connection between integrated structures is modelled. Three methods are investigated in this paper: shared nodes, coincident nodes and sliding surfaces.

#### 2.1.1. Geometry

Two panel geometries have been modeled. Panels 1.1 and 1.2 are used to establish the final dimensions to be used. Panel 1.1 is 1100 mm in length and 700 mm in width when panel 1.2 is 870 mm in length and 509 mm in width. Other models have a geometry of 870 mm in length and 509 mm in width.

#### 2.1.2. Panel model

Fig. 1 shows how the composite stiffened panel is defined. A parametric convergence study has allowed the number of elements to be defined for each geometric entity of a representative 2D shell model made of CQUAD4 elements. The mesh density has been obtained for the 20 first buckling eigenvalues of all integrated structure areas to be converged. Since the first buckling modes are located at the panel skins, other modes have to occur in the integrated structure areas. This work with Patran integrated scripts is not detailed here and leads to define in the presented models a minimum number of five elements at the hat shaped stringer's webs and six elements at the top. Obviously the number of elements in the stringers' length is related to the number of elements in the stringers top and webs. Furthermore, to insure the accuracy of the models on local strains, the radius were modeled between webs and flanges, top and webs and transverse integrated structures and skins.

**Table 1**
Characteristics of the presented models

| Analysis | Reference number | Boundary condition | Geometry (mm × mm) | Material properties | Connection method |
|---|---|---|---|---|---|
| Linear buckling | 1.1 | $F = 1N$ | 1100 × 700 | Table 2 | Shared nodes |
| | 1.2 | | 870 × 509 | | |
| Linear statics | 2.1 | $F = 50$ kN | 870 × 509 | Table 2 | Shared nodes |
| | 2.2 | $F = 400$ kN | | | |
| | 3.1 | $UX = -4$ mm | 870 × 509 | Table 2 | Shared nodes |
| Geom. NL | 3.2 | | | | Coincident nodes |
| MARC | | | | | |
| SOL600 | 3.3 | | | | Sliding surfaces |
| Geom. NL | 4.0 | $UX$ | 870 × 509 | Mean | Coincident nodes |
| MARC | 4.1 | $= -4$ mm | | Low | |
| SOL600 | 4.2 | | | High | |

*2.1.3. Boundary conditions*

With the help of 2 Rigid Body Elements Form 2 (RBE2), all degrees of freedom (dof) 123456 are constrained since one edge of the panel is clamped, while the second edge is free to move in the axial direction only dof 23456 are constrained. Fig. 2 displays the modelling of the panel.

Two grid points are defined as independent grid points, transmitting corresponding dof to the dependant nodes located at the panel edges. Load at the loaded edge (see Fig. 1) is a boundary condition which depends on the analysis type. The modelling strategy between each referenced model is outlined in Fig. 3, it underlines the use of results obtained by each analysis type to be introduced in the next one.

For linear buckling in Nastran SOL105, a unit load is applied to the independent grid point. Then the calculated eigenvalue $\lambda$ points to the minimum force to be applied to this grid point in a linear static analysis in Nastran SOL101. This linear static analysis is aimed at easily obtaining the panel shortening at failure, to be incorporated in a non linear analysis. Finally, by increasing the applied force until failure, the independent grid point displacement is recorded and used in the non linear solver Marc to consider geometric non linearity, called by SOL600 in Nastran. A displacement of 4 mm is applied at the independent node and incremented to obtain 0.05 mm steps.

Also three connection methods between longitudinal stiffeners and transverse structures were investigated. A detailed view of the mesh at their intersection (see (c) in Fig. 2) is the area where these conditions are studied. In reality panels that have already been manufactured contain a space between these two intersecting structures which is filled by resin. These two structures are integrated by infusing them at the same time as the skin of the panel. For numerical modelling purposes, several approaches are compared. Shared nodes means that adjacent elements share their nodes on the contact line. Coincident nodes means that each adjacent element on the contact line has its own node that can move independently. Then sliding surfaces are defined between surfaces containing these coincident nodes, which means that they are restrained to move inside elements contained in adjacent surfaces (they can move apart but can not penetrate). The resin itself is not modelled as the stiffness of this resin gap is neglected in these analyses.

*2.2. Material properties*

G0926/RTM6 is a five harness satin carbon fibre woven fabric, manufactured by LRI with RTM6 epoxy resin. Its material properties are taken from Hexcel [18] and are given in Table 2. Warp and weft directions are considered equivalent. From industrial feedback a Poisson's ratio of $\nu_{LT} = 0.05$ is admitted as being representative of a G0926/RTM6 fabric. $E_L$ and $E_T$ stand for the longitudinal and the transverse Young moduli respectively, and $G_{LT}$ for the shear modulus. $X$ and $Y$ denote the strength in the longitudinal and the transverse directions, in tension (indice $T$) and in compression (indice $C$). $S_{12}$ is the in-plane shear strength.

In the end panel behaviours will be compared to those using industrial material properties.

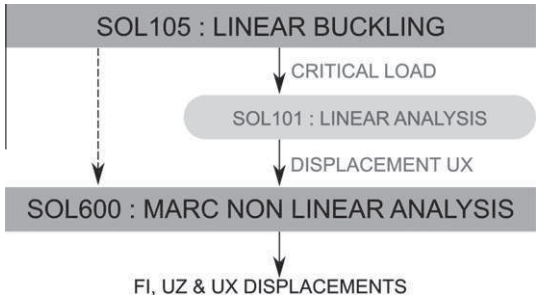


**Fig. 3.** Modelling strategy between each analysis.

**Table 2**
G0926/RTM6 properties from Hexcel–Ply thickness is 0.37 mm for a fibre volume fraction of $V_f = 60\%$, dry/room temperature [18,19]

| Property | Mean (MPa) |
|---|---|
| $E_L = E_T$ | 60,000[a] |
| $G_{LT}$ | 4300 |
| $X_T = Y_T$ | 860 |
| $X_C = Y_C$ | 700 |
| $S_{12}$ | 100 |
| $\nu_{LT}$ | 0.05 |

[a] Compression Young modulus is used

## 3. Results and discussion

*3.1. Linear buckling – SOL105*

The first five eigenvalues $\lambda$ are calculated by the Lanczos method. Fig. 4 shows eigenvectors and the corresponding eigenvalues defining the critical buckling load $F_{cr}$ for two panel geometries.

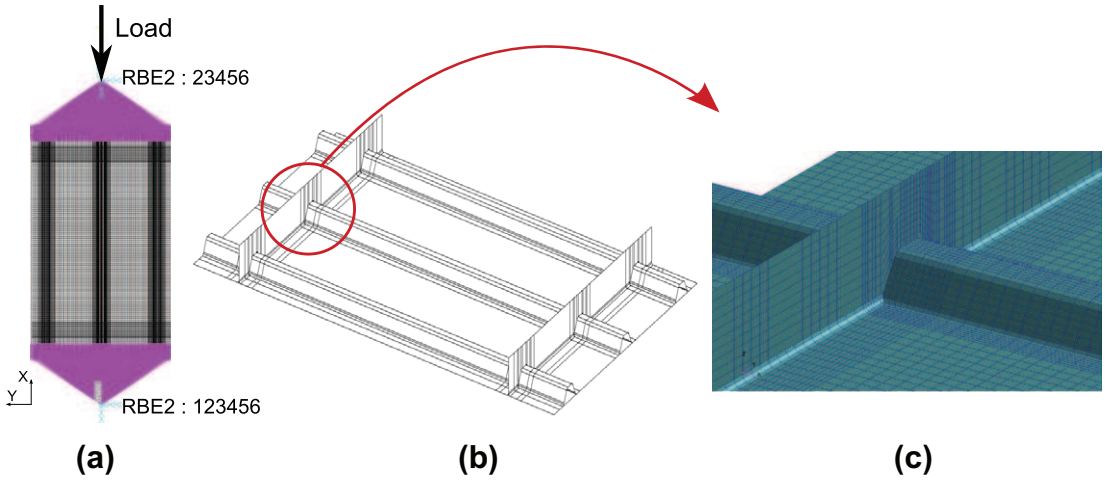


**Fig. 2.** Modelling of the composite stiffened panel. (a) RBE2s on the model and the load, (b) whole isometric view of the model and (c) detailed view of the mesh.

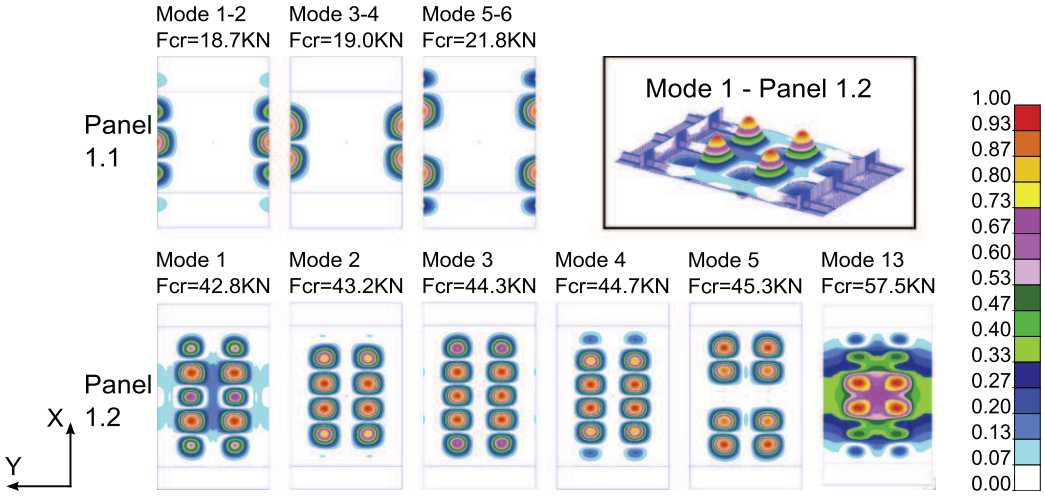


**Fig. 4.** Linear Buckling mode shapes.

Also mode 1 of panel 1.2 is framed to underline the shape of the panel when it buckles. Linear buckling analysis provides a quicker method to analyse the expected shape of the panel during loading and then to set appropriate boundary conditions.

### 3.2. Linear analysis – SOL101

The Tsai–Wu criterion [15] given in Eq. (1) has been implemented with an arbitrary interaction term $F_{12} = -0.5$ for a usual plane stress formulation. $\sigma_1$ and $\sigma_2$ are stresses in the longitudinal and transverse directions of the ply. $\tau_{12}$ is the shear stress. $T$ and $C$ indices stand for allowable tensile and compressive stresses respectively in the warp ($X$) and weft ($Y$) directions. 12 indice is for shear. The Tsai–Wu failure criterion is an interactive failure criterion. It does not give the mode of failure but includes stress interactions. This makes it convenient to study a global behaviour of a part as all failure modes are included in one expression.

$$\left(\frac{1}{X_T}-\frac{1}{X_C}\right)\sigma_1+\left(\frac{1}{Y_T}-\frac{1}{Y_C}\right)\sigma_2+\frac{\sigma_1^2}{X_T X_C}+\frac{\sigma_2^2}{Y_T Y_C}+\left(\frac{\tau_{12}}{S_{12}}\right)^2 + 2F_{12}\sigma_1\sigma_2 \quad (1)$$

Four configurations have been calculated using approximately the first critical force of 50 kN for skin buckling found in linear buckling analysis with panel 1.2 (as shown in Fig. 4). Fig. 5 shows results of panels 2.1 and 2.2 with a similar range for each result, for a force of 50 kN and 400 kN respectively.

Displayed results are $X$ displacements along the panel length in (a), $Z$ displacements which are the out of plane displacements during the linear stage in (b), and finally Failure Indices (FI) in (c) as

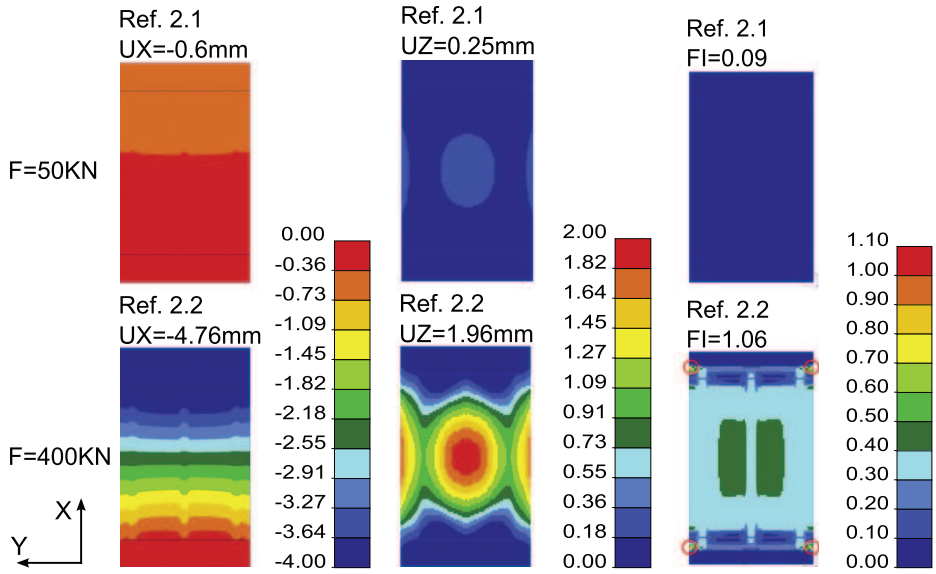


(a) Displacements on X (longitudinal shortening)

(b) Displacements on Z (out of plane displacements)

(c) Tsai-Wu failure indices

**Fig. 5.** Linear analysis results for panels 2.x.

indicated in Eq. (1). FI must be smaller than 1 for the structure to remain safe.

### 3.3. Linear results

In Fig. 4 the first six buckling modes of panel 1.1 (with the largest width) can be put together in pairs as these pairs of modes are equivalent. They show that skin areas at panel edges can buckle thus leading to a catastrophic failure initiated from these areas which is not what is expected. Comparing this with panel 1.2 shows that reducing the panel width for the side stiffeners to be located at panel borders, avoid failure to be initiated on the edges. In other terms, reducing skin areas on the longitudinal edges suppresses edge buckling modes.

Indeed by decreasing the panel dimensions for the width to comprise at least the whole flanges of the lateral stiffeners (panel 1.2) it can be seen that the previous observed edge modes on panel 1.1 do not occur anymore. The first five modes correspond to skin buckling, the first one showing the first expected skin buckling mode shape at around 43 kN. The first global buckling mode is the thirteenth one, other previous modes all being skin buckling modes. As a result the buckling mode shape to appear is a skin buckling mode at 43 kN, and the structure should buckle globally from approximately 57 kN. As it can be seen the first buckling mode is a skin symmetric mode with five waves on each skin. Each wave pair on both skins are either positive or negative as seen in the framed picture.

Looking at linear analysis results with SOL101 in Fig. 5 it can be noticed that the panel 2.1 has $FI = 0.09$ and that it is safe at 50 kN. For the panel to collapse, the load to be applied raises to 400 kN for $FI = 1.06$. Stresses concentrate at panel end borders where FI is the highest. The longitudinal displacement of $UX = -4.76$ mm is written down to be further introduced in the non linear analysis. In fact a shortening of $UX = -4$ mm will be applied as it is obvious that shortening at collapse is less with geometric non linearity taken into account.

The value of 400 kN for the load to collapse the panel is much larger than the global buckling load. Then it can be said that a linear analysis does not permit to study the failure. Indeed the linear analysis can only be used for failure up to the first buckling point, after which the results are meaningless, because the buckling shape will totally change the panel behaviour.

### 3.4. Geometric non linearity – Marc with SOL600

A progressive failure behaviour is implemented using MATF entry in the Nastran card. The material is linear elastic defined by its orthotropic properties (see Table 2). The Tsai–Wu criterion is used to calculate the element failure state at each ply. When the criterion reaches a value of 1, the element is considered to have failed by reducing all material moduli at the integration point to the lowest modulus specified [20].

Fig. 6 shows load shortening curves to be compared between panel 3.1, 3.2 and 3.3. Reaction force and longitudinal displacements are extracted from the independent node where incremental displacement is controlled, being the load and the shortening respectively.

Also three noticeable stress states are shown in Fig. 7 using Tsai–Wu FI for the three studied connection methods. These are a pre-failure state for one increment preceding failure, a post failure state at which Tsai–Wu FI reaches 1 and a collapsed state when the load has so significantly decreased, it can be considered that the whole structure has collapsed.

Fig. 8 shows displacements being picked up at the nodes located at the central stiffener–transverse structure intersection, for coincident nodes configuration. Node displacements along the $Z$ axis

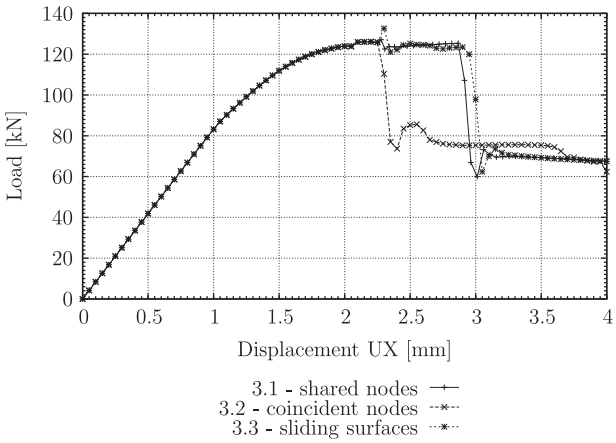


**Fig. 6.** Load shortening curves for three connection methods.

of the stiffener intersecting elements have been compared with nodes belonging to the transverse structure elements. Obviously only one value can be obtained for panel 3.1 as nodes are shared.

Given the load levels found in the load shortening curves shown in Figs. 6, 9 gives their corresponding out of plane displacements. Displays are ordered according to noticeable load levels of the load shortening curve. The first one is the linear–non linear transition with three images being displayed to see the transition at approximately 87 kN (as shown in Fig. 9a). A load step seen between 124 kN and 126 kN is also represented by two images for each panel (as shown in Fig. 9b). Then a load peak is only present on panel 3.1 and 3.3 near 125 kN (as shown in Fig. 9c). In fact, panel 3.2 shortening at collapse corresponds to this load peak, and is represented along with panels 3.1 and 3.3 in Fig. 9d.

### 3.5. Geometric non linear results

First of all, it is seen that in Fig. 7 the three panels pre-failure states are the same depending on the connection method at a load of 125 kN and a longitudinal displacement of $UX = 2.25$ mm. Looking at Fig. 6 it means that their load evolution until the collapse of panel 3.2 are similar. Now coming back to Fig. 7, coincident nodes and sliding surface connection methods (as shown in (b) and (c) respectively) have skin failure contrary to what is seen in (a) which shows end stiffener failure only for shared nodes (panel 3.1) at a higher longitudinal displacement (2.91 mm for panel 3.1 versus 2.30 mm for panels 3.1 and 3.3). As the intersection is rigidified by shared nodes between adjacent elements, it seems that they do not allow the panel to fail in the central stiffener region surrounded by two skin failures (as seen in (b) and (c)). Indeed collapse of panel 3.1 takes the form of stiffener end failure. For panel 3.2 as for panel 3.3 skin failure occurs followed by stiffener end failure. Behaviour of these two panels differs a little in the failed areas: panel 3.2 has skin failure on each skin as well as central stiffener failure, when panel 3.3 has only skin failure. Furthermore the longitudinal displacement leading to collapse is different, being 2.45 mm for panel 3.2 and 3.05 mm for panel 3.3.

Buckling load evolution on load shortening curves can be ideally described with three marked load levels [21], the first local buckling load being the skin buckling between the stiffeners, then the first global buckling load being governed by the stiffener load carriage capacity, finally leading to the collapse load which is the highest load. This sequence of mechanisms has been originally elaborated for describing the global behaviour of the debonding of prepregs composite panels made of co-bonding structures. Results of displacements and FI illustrated in Fig. 6 could be described using this sequence.

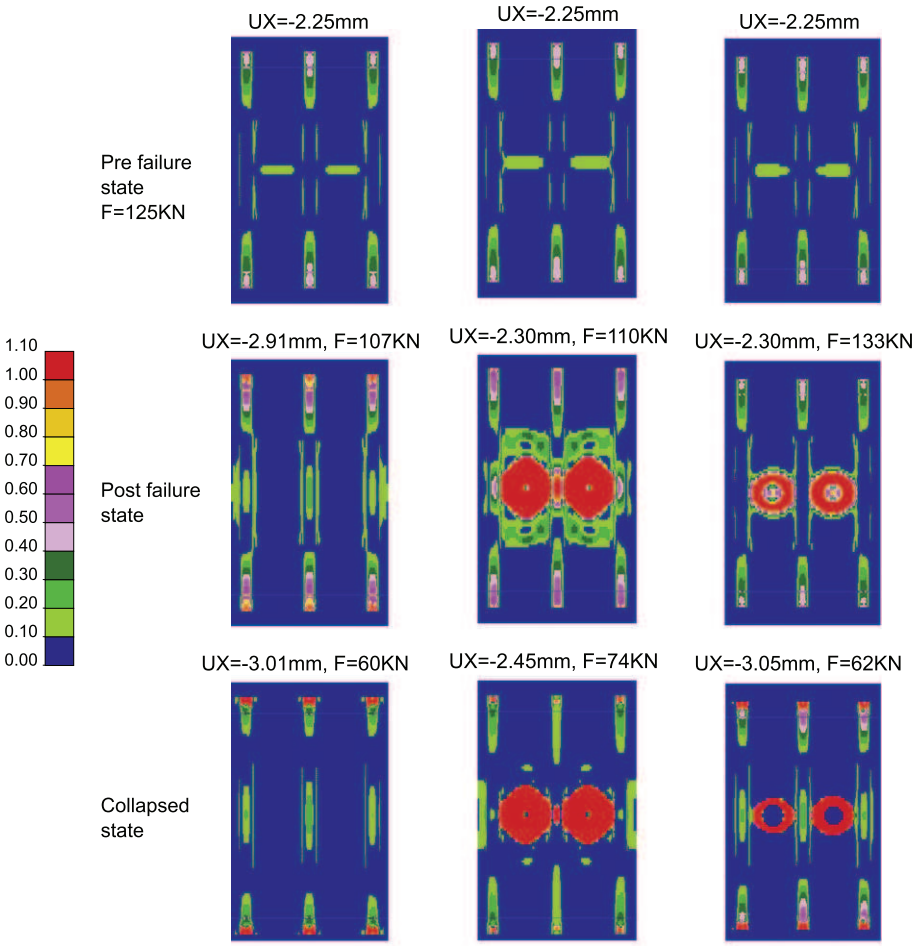


(a) Panel 3.1: shared nodes (b) Panel 3.2: coincident nodes (c) Panel 3.3: sliding surfaces

**Fig. 7.** Tsai–Wu Failure Indices results for a progressive failure analysis comparing different connection methods at intersection, at three load levels.

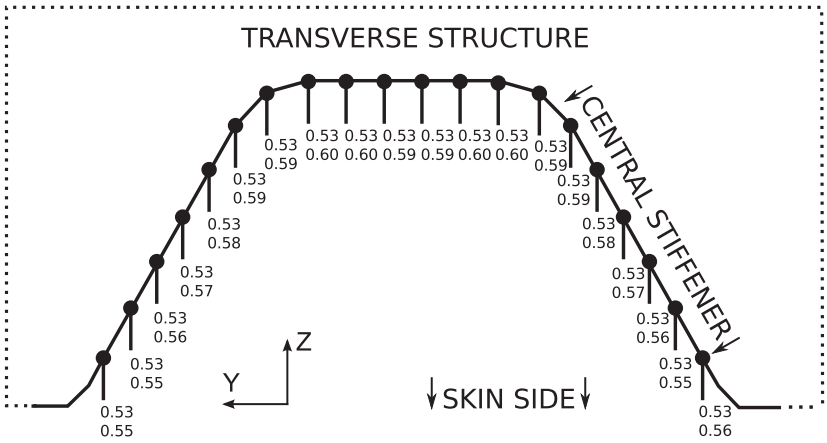


**Fig. 8.** Displacements of the nodes [mm] at the intersection of the stiffeners and the transverse structures. Panel 3.2 with coincident nodes.

Numerical results as seen in Fig. 9a show that global buckling occurs during the linear stage. It is followed by local skin buckling which is mixed with global buckling. This sequence is not concordant with the given description of the buckling mechanism [21]. That can be explained first by the flat shape of the studied panel which leads the panel to buckle globally on the stiffener side, plus no gliding conditions on the longitudinal edges of the panels. In addition, the buckling shape totally changes the panel behaviour. Then consideration of the small displacements corresponding to eigenvectors would improve the non linear results once the buckling load is achieved. In fact the linear analysis is meaningful only until the first buckling load. An experimental study will permit to compare numerical and experimental results.

Nevertheless, the buckled panel shows mixed skin global buckling once the second load level is achieved. This can be seen in Fig. 9a for the three connection methods where the panel is buck-

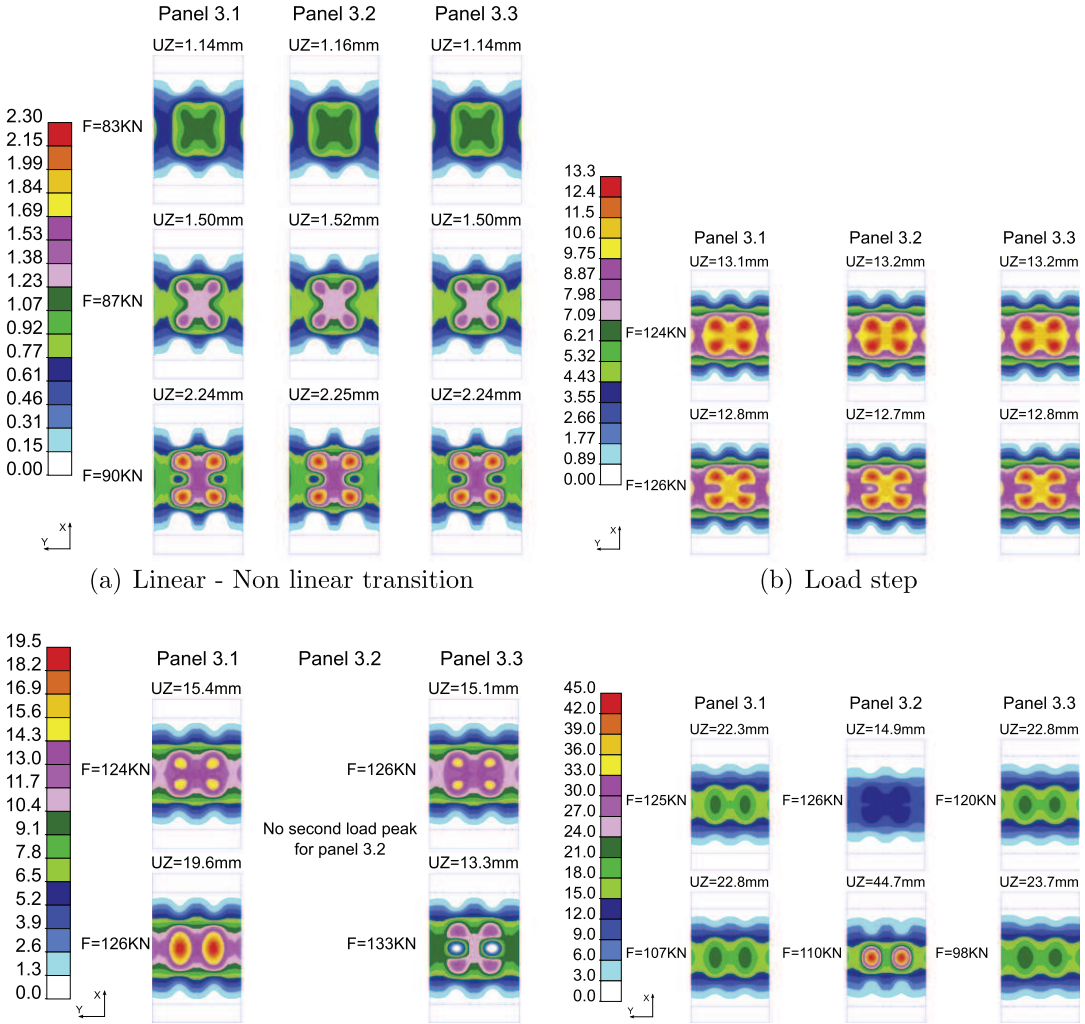


**Fig. 9.** Out of plane displacements for three connection methods: Panels 3.1, 3.2 and 3.3.

led globally at 83 kN, followed by the linear–non linear transition at 87 kN. At 90 kN out of plane displacement field of all panels consists of five symmetric waves as found in the linear buckling analysis shown in Fig. 4.

Until the load step (defined by Fig. 6 at 2.1 mm shortening), the central negative wave is being reduced. Panels are represented by the 124 kN images of Fig. 9b. The load step seems to be induced by the central negative wave re-formation as it can be seen on the second image at 126 kN where the central negative wave becomes larger. A higher load is then necessary for the skins to keep buckling.

Same observations can be made for the central wave evolution as it is being reduced again until the load peak defined by Fig. 6 at 2.25 mm shortening. The load peak of panels 3.1 and 3.3 (see Fig. 9c) is not caused by the same phenomenon. For panel 3.1 a global central wave is formed on each skin from three waves, while for panel 3.3 a central negative wave is created again. This would be attributed to the rigidity supplied by the shared nodes connection method as it makes it difficult for another skin buckling wave to be created. Then it can be said that the panel 3.3 has a contact configuration halfway between panels 3.1 and 3.2.

Failure of panel 3.2 arises at the same load and displacements as panels 3.1 and 3.3 in Fig. 9c, but its failure image is given in Fig. 9d because panel 3.2 collapses together with first ply failure instead of showing a load peak. As seen before in Fig. 7, panel 3.1 collapses with failure at stiffener ends and there is no noticeable difference in its out of plane displacement field between both images in Fig. 9d. Panel 3.2 collapses as the skins and the central stiffener fail. It can be seen a central skin buckling shape is created on each skin. No node displacements are restrained at the intersection between the stiffeners and the transverse structures. That seems to be the reason why stresses concentrate more at stiffener ends for panels 3.1 and 3.3 in Fig. 7. In fact the out of plane displacement of 44.7 mm for panel 3.2 is reduced in the same order as for panel 3.1 and 3.2 when looking at their collapsed state at around 3 mm shortening.

Finally panel 3.2 directly collapses before the load peak without stresses being concentrated at stiffener ends, contrary to panel 3.1 and 3.3. As this is a progressive failure analysis, skins would not carry load anymore once they have failed since failed elements have their properties reduced (cf. Section 3.4). So if skin–stiffener failure is experimentally observed, skins and the central stiffener will be failed at panel collapse and the out of plane displacement of 44.7 mm will not be as much as what is found in this analysis.

### *3.6. Influence of the connection method between integrated structures*

The main differences concern the shortening value before collapse. It seems panel 3.1 (shown in Fig. 7a) is too rigid at its

intersections due to its shared nodes between two adjacent elements. Taking into account coincident nodes on panel 3.2 seems to annihilate this effect. Indeed, intersections are softened and failure does not occur anymore, but occurs in the central stiffener and skin areas. Considering panel 3.3 and sliding surfaces for adjacent element nodes to not penetrate each other, the failure always occurs at the central skins but not in the central stiffener area. It permits the failure to always occur at the central skins but not in the central stiffener area. It is also followed by stiffener ends failure. Node displacements in the contact region are compared in the next section.

### 3.7. Node displacements at stiffener–transverse structure intersections

While error in displacements for sliding surfaces has been calculated to less than 2% for all nodes, it reaches 11% when considering some coincident nodes shown in Fig. 8. During the manufacturing process the small space between stiffeners and transverse structures is filled with resin. The two surfaces are not really in contact with each other. Displacement gaps between two coincident nodes have been calculated and are small (less than 0.07 mm). As seen for panel 3.2, the panel collapses as soon as first ply failure occurs because no more load is carried by the stiffener ends. This observation concords with panels 3.1 and 3.3 which can sustain a higher displacement as seen in Fig. 6. Since in reality stiffeners and transverse structures are not really in contact, a larger gap exists – larger than the maximum calculated gap of 0.07 mm – which is a resin fillet unable to carry any load. In such a case it can be said it is not necessary to use sliding surfaces. Moreover it is simpler in this analysis to consider coincident nodes and permit their penetration inside adjacent elements, rather than to model a small space between adjacent surfaces. Panels 4.0, 4.1 and 4.2 are then modeled with coincident nodes.

### 3.8. Comparison with industrial material properties

As the connection method of the panel 3.2 seems to be the most representative (see Section 3.7), this model is kept for introducing other material property data entries. The results obtained from Table 2 are then compared to the same models using industrial material properties. Load shortening curves are drawn in Fig. 10.

Methods to obtain load and displacement results are similar to what has been explained in Section 3.4. There are three property data sets used in panels 4.x models. It is not possible to give the material data sets in this study as these are treated confidentially. The properties used for mean properties are obtained from a set of design allowables, which is used to substantiate the finite element models. The two other sets come from the low and high properties calculated from the standard deviation of each property.

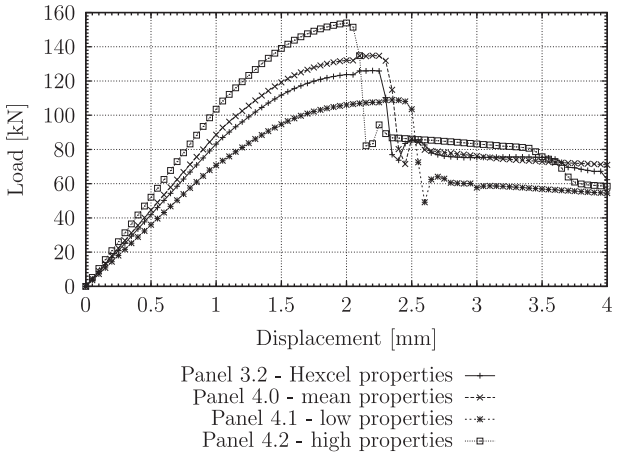


**Fig. 10.** Load shortening curve of panel 3.2 compared to the same panel using industrial properties.

### 3.9. Global behaviour of the panel to be tested

The first observation is that the behaviours of panels 3.2 and 4.0 are relatively close to each other, showing that using Hexcel material properties is a good approach for modelling these composite stiffened panels manufactured by LRI. There is approximately a 10 kN difference when curves of panels 3.2 and 4.0 reach the load plateau. The slope of the curves in the linear phase represents the global rigidity of each panel. As expected, the higher the Young modulus is and the higher the slope of the curve is.

Load step is observed on panels 4.0 and 4.1 only, as explained with Fig. 9 in Section 3.5 where the step seems to originate from the central wave re-formation. Panel 4.2 fails at stiffener ends without showing a load step. It is likely caused by too much rigidity as with what has been seen with panel 3.1 where stresses concentrate at stiffener ends.

Collapse of panel 4.0 appears a bit further in displacement than panel 3.2, which is not in concordance with the curves of panels 4.1 and 4.2 compared to the curve of panel 3.2. Indeed, it can be seen that the higher the properties are, the less displacement there is at collapse. After collapse all curves are stored in the same order as their global rigidity. An experimental investigation of this composite stiffened panel in compression is needed to compare more precisely the differences between these curves. However these numerical curves indicate the load shortening of the expected global behaviour of the panel to be tested.

Curves of panels 4.1 and 4.2 provide tolerance intervals, for the analyses carried out during this study to be verified experimentally.

## 4. Conclusions

The presented numerical analyses (see Table 1) study the global behaviour of a composite stiffened panel infused with integrated structures in two directions. Collapse of the panel is undertaken using a progressive failure analysis.

At the global scale of the composite stiffened panel, the stacking sequence is considered a whole structure at the skin–stiffener interface. Moreover, as the panel is manufactured by LRI to integrate structures and since its global behaviour is studied, no interface is considered for debonding. The Tsai–Wu stress criterion has been implemented inside a progressive failure analysis with moduli being reduced at each element once failure occurs. Load shortening curves are obtained and give the expected level of load to be used for the design of an experimental test. A longitudinal load of 120 kN can be expected as well as a shortening to collapse in the range of 2–2.5 mm.

Also the boundary conditions corresponding to an experimental test have been investigated. One clamped edge and one edge to apply a displacement and measure the load have been defined in the numerical models. These boundary conditions are realistically feasible on a test machine, and side border gliding conditions do not seem to be mandatory. It has also been seen that modifying connection methods between several structures considerably influences the collapse of the panel. It has been seen that considering coincident nodes at their intersection permits to not overconstrain

the panel. The skin–stiffener interface and its local behaviour will be studied from observations of the experimental investigation.

However for a panel in compression it has been noticed that debonding of the stringer is not the source of the post-buckling failure for a prepreg co-cured stiffened panel [12], whereas it has been observed on a co-bonded stiffened panel at the element level [5] and it is combined with delaminations and fractures in the skin and the stringer flanges at the panel level [4,17]. As a distinct bonded interface is missing, panels manufactured by LRI from dry fabrics are intended to be a little different from those manufactured from co-bonded and co-cured structures made of prepregs. However, discontinuities at the skin–stringer interface and at the stringer termination still exist. In all previous studies, these locations are areas of stress concentrations and are considered the source of delaminations. The failure mechanisms occuring at these locations have to be investigated locally by numerical models and experimental tests. For example three dimensional detailed finite element models would allow a deeper study of the cohesive failure mechanism (offsets in shell elements are not used in these analyses). Then it appears necessary to question how a debond of the skin–stiffener would appear on a representative detailed model (i.e. with the displacement field corresponding to a global model representing a real stress case). Experimental investigation of full-size composite stiffened panels will permit to highlight failure mechanisms to be correlated with these global models and then enhance them. Furthermore this will allow building more precise local models based on the studied global models.

One important drawback is to use initial displacements of the first buckling mode in a first load level for the local skin buckling to occur before global buckling, even if it has been seen the calculated mixed skin global mode which appeared during loading is realistic.

Finally models with Hexcel material properties are quite close to models using mean industrial properties and then it can be said the real behaviour of the studied panel should be comprised between models with low and high industrial properties. Model robustness is an aspect which is not dealt with, depending primarily on the material properties used as input data. In this study only low and high properties have been introduced into models, but other uncertainties exist, for example, related to real boundary conditions which are in all cases difficult to assess.

## References


[1] Fielder L, Barr S, Molina J, Voto C. Tango composite fuselage platform. SAMPE J 2003;39(1):57–63.

[2] Zimmermann R, Rolfes R. Posicoss – improved postbuckling simulation for design of fibre composite stiffened fuselage structures. Compos Struct 2006;73:171–4.

[3] Degenhardt R, Rolfes R, Zimmermann R, Rohwer K. Cocomat material exploitation of composite airframe structures simulation of postbuckling and collapse. Compos Struct 2006;73:175–8.

[4] Orifici A, Thomson R, Degenhardt R, Kling A, Rohwer K, Bayandor J. Degradation investigation in a postbuckling composite stiffened fuselage panel. Compos Struct 2008;82(2):217–24.

[5] Orifici A, Alberdi I, Thomson R, Bayandor J. Compression and post-buckling damage growth and collapse analysis of flat composite stiffened panels. Compos Sci Technol 2008;68:3150–60.

[6] Tay T, Tan S, Tan V, Gosse J. Damage progression by the element-failure method (efm) and strain invariant failure theory (sift). Compos Sci Technol 2005;65:935–44.

[7] Rybicki E, Kanninen M. A finite element calculation of stress intensity factors by a modified crack closure integral. Eng Fract Mech 1977;9:931–8.

[8] Krueger R. Virtual crack closure technique: history, approach and applications. Appl Mech Rev 2004;57:109–43.

[9] Benzeggagh M, Kenane M. Measurement of mixed-mode delamination fracture toughness of unidirectional glass/epoxy composites with mixed-mode bending apparatus. Compos Sci Technol 1996;56(4):439–49.

[10] Bertolini J, Castanié B, Barrau JJ, Navarro JP. An experimental and numerical study on omega stringer debonding. Fourteenth international conference on composite structures – ICCS/14. Compos Struct 2008;86(1–3):233–42.

[11] Bertolini J, Castanié B, Barrau JJ, Navarro JP. Multi-level experimental and numerical analysis of composite stiffener debonding. Part 1: Non-specific specimen level. Compos Struct 2009;90(4):381–91.

[12] Bertolini J, Castanié B, Barrau JJ, Navarro JP, Petiot C. Multi-level experimental and numerical analysis of composite stiffener debonding. Part 2: Element and panel level. Compos Struct 2009;90(4):392–403.

[13] Krueger R, Minguet P. Analysis of composite skin–stiffener debond specimens using a shell/3d modeling technique. Compos Struct 2007;81:41–59.

[14] Krueger R, Ratcliffe JG, Minguet PJ. Panel stiffener debonding analysis using a shell/3d modeling technique. The sixteenth international conference on composite materials with regular papers. Compos Sci Technol 2009;69(14): 352–62.

[15] Tsai SW, Wu EM. A general theory of strength for anisotropic materials. J Compos Mater 1971;5:58–80.

[16] Ambur DR, Rouse M. Design and evaluation of composite fuselage panels subjected to combined loading conditions. J Aircraft 2005;42(4):1037–45.

[17] Zimmermann R., Klein H., Kling A. Buckling and postbuckling of stringer stiffened fibre composite curved panels – tests and computations. International Conference on Buckling and Postbuckling Behavior of Composite Laminated Shell Structures. Composite Structures 2006;73(2): 150–61.

[18] Hexcel. Hexflow rtm6 product datasheet. 2010a.

[19] Hexcel. Hexforce g0926 d 1304 tct inj e01 2f product datasheet. 2010b.

[20] MD Nastran R3 Quick reference guide. Organization MSC Software Corporation; 2010.

[21] Degenhardt R, Kling A, Rohwer K, Orifici A, Thomson R. Design and analysis of stiffened composite panels including post-buckling and collapse. Comput Struct 2008;86(9):919–29.